View metadata, citation and similar papers at core.ac.uk
brought to you by CORE
provided by RMIT Research Repository

Thank you for downloading this document from the RMIT Research Repository.

The RMIT Research Repository is an open access database showcasing the research outputs of RMIT University researchers.

RMIT Research Repository: http://researchbank.rmit.edu.au/

Citation:

Castelletto, S, Johnson, B, Ivady, V, Stavrias, N, Umeda, T, Gali, A and Ohshima, T 2013, 'A silicon carbide room temperature single-photon source', Nature Materials, pp. 1-6.

See this record in the RMIT Research Repository at:

http://researchbank.rmit.edu.au/view/rmit:22805

Version: Accepted Manuscript

Copyright Statement: © Macmillan Publishers Limited. All rights reserved.

Link to Published Version:

http://dx.doi.org/10.1038/nmat3806

PLEASE DO NOT REMOVE THIS PAGE

A Silicon Carbide Room Temperature Single Photon Source

S. Castelletto,[1,*] B. C. Johnson,[2,3] V. Ivády,[4,5] N. Stavrias,[6] T. Umeda,[7] A. Gali,[4,8] and T. Ohshima[3]

[1]*School of Aerospace, Mechanical and Manufacturing Engineering RMIT University, Melbourne, Victoria 3001, Australia*

[2]*Centre for Quantum Computation and Communication Technology, School of Physics, University of Melbourne, Victoria 3010, Australia*

[3]*SemiConductor Analysis and Radiation Effects Group, Japan Atomic Energy Agency, 1233 Watanuki, Takasaki, Gunma 370-1292, Japan*

[4]*Institute for Solid State Physics and Optics, Wigner Research Centre for Physics, Hungarian Academy of Sciences, Budapest, POB 49, H-1525, Hungary*

[5]*Department of Physics, Chemistry and Biology, Linköping University, SE-581 83 Linköping, Sweden*

[6]*School of Physics, University of Melbourne, Victoria 3010, Australia*

[7]*Graduate School of Library, Information and Media Studies, University of Tsukuba, Tsukuba 305-8550, Japan*

[8]*Department of Atomic Physics, Budapest University of Technology and Economics, Budafoki út 8, H-1111, Budapest, Hungary*

Abstract

Over the past few years, single photon generation has been realized in numerous systems: single molecules[1], quantum dots[2–4], diamond colour centers[5] and others[6]. The generation and detection of single photons play a central role in the experimental foundation of quantum mechanics[7] and measurement theory[8]. An efficient and high-quality single-photon source is needed to implement quantum key distribution, quantum repeaters and photonic quantum information processing[9]. Here we report the identification and formation of ultra-bright, room temperature, photo-stable single photon sources in a device-friendly material, silicon carbide (SiC). The source is composed of an intrinsic defect, known as the carbon antisite vacancy pair, created by carefully optimized electron irradiation and annealing of ultrapure SiC. An extreme brightness (2×10^6 counts/s) resulting from polarization rules and a high quantum efficiency is obtained in the bulk without resorting to the use of a cavity or plasmonic structure. This may benefit future integrated quantum photonic devices[9].

Silicon carbide (SiC) is an important wide-band-gap semiconductor for high-power electronics, high-temperature applications and is a key material for next generation photonic[10] and electronic devices[11]. As such, SiC has well-established growth and device engineering protocols[12], and 3 inch ultra-pure wafers are now commercially available. This has allowed the development of a mature platform for nano-fabrication and high-Q photonic crystal cavities, reported for a spectral region from 550 to 1450 nm[10] as well as microdisk resonators[13] for cavity opto-mechanical applications. In addition, SiC is also bio-compatible, especially to blood and SiC nano-particles (quantum dots) have been employed as fluorescent biological labels in cell imaging[14,15].

Recently, it has been indicated[16–20] that SiC could harbor defects that may be employed as solid-state qubits. The existence of such defects in a device-friendly material is extremely fortuitous and holds great promise for the future implementation of scalable quantum processors[17,21]. Ensembles of candidate optically-active defects, having the net angular momentum (or spin) required to act as qubits operating at room temperature, have already been identified in SiC[18–20]. Their optically detected magnetic resonance has a lower visibility compared to the NV center in diamond. However, the richness of possible defects in the various polytypes of SiC[20] will enable further studies and discoveries. Presently, a major challenge before the future deployment of this material in the field of quantum technologies, is to identify and form isolated defects.

In this work, we present, to the best of our knowledge, the first observation and engineering of an isolated defect in SiC that exhibits single photon emission. To isolate single defects and identify them, we irradiated ultrapure SiC with low electron doses and we optimized the annealing temperature to increase/decrease the number of defects created from the single to the ensemble level. This approach allows the direct correlation between ensemble and single defects, otherwise often difficult. The emission rate of this single photon source is in the Mcounts/s regime, the brightest single photon in bulk material at room temperature. In comparison, Cr-related centers in bulk diamond yield a single photon count rate of 0.7 Mcounts/s[22]. Only Cr-related and Silicon vacancy centers in nanodiamonds can yield emission rates above 3-4 Mcounts/s[23,24] although for the latter case enhancement of the spontaneous emission count rate arose from plasmonic effects due to a metal substrate. A maximum emission rate of 1-2 GHz for NV centers in nanodiamonds can be achieved using a solid immersion lens to enhance the collection efficiency although with higher pump powers

the NV center is prone to blinking[25]. The SiC single photon source has several zero phonon lines (ZPLs) and so is expected to display efficient cavity coupling at low temperatures. Presently, the brightest solid-state single photon sources are based on advanced fiber-coupled microcavity-InAs/GaAs-quantum dots, reaching GHz repetition rate single photon emission at 4 K[26]. Further development of single photon emission in SiC nanoparticles are expected to provide similar rates. Our work together with the possibility of nano-structuring this material will pave the way for further studies on the spin and charge state of this defect as well as quantum emitters in this emerging material.

High purity, semi-insulating 4*H*-SiC wafers were irradiated with high energy electrons to different fluences to create defects and then annealed at various temperatures (see Methods for details). This method allows the creation of defect densities from the single isolated level to the ensemble level.

To identify the defect, ensemble room temperature and low temperature photoluminescence (PL) measurements were performed with 532 nm excitation on a sample irradiated to a fluence of 10^{17} e/cm^2. At 80 K the so-called AB lines[27] can clearly be observed with lines at A1=648.7 nm, A2=651.8 nm, B1=671.7 nm, B2=673.0 nm, B3=675.2 nm, and B4=676.5 nm as indicated in Fig. 1a. These lines arise from the carbon antisite-vacancy pair defect, $C_{Si}V_C$[28]. We also resolve two additional peaks at A3=665.1 nm and A4=668.5 nm which we assign to the same defect. The atomistic model of the $C_{Si}V_C$ with its four possible cubic or hexagonal orientations is shown in the inset of Fig. 1a.

A study on the effect of the measurement and annealing temperature on the AB lines (Fig. 1(b,c)) revealed the onset of thermal quenching at around 150 K and the enhancement of AB lines on annealing up to 800°C. These measurements are compared to the silicon vacancy defect, V_{Si}[29], which gives rise to the V1/V2 PL lines at 861.5 and 916.3 nm, respectively (see details in Supplementary). Here it is observed that the AB lines grow at the expense of V1. At the temperature at which the AB lines are optimized the V1/V2 system is almost absent. Such behaviour is supported by ab-initio calculations where it has been shown that the energy barrier to formation of $C_{Si}V_C$ from V_{Si} is small and is promoted by an increase in the annealing temperature[30]. As will be shown, this has a large positive impact on the photo-stability of the $C_{Si}V_C$ at the single defect level.

Ab-initio supercell calculations on the $C_{Si}V_C$ defect in 4*H*-SiC in conjunction with group theory was employed to describe the AB PL spectra (see Supplementary). A schematic of the

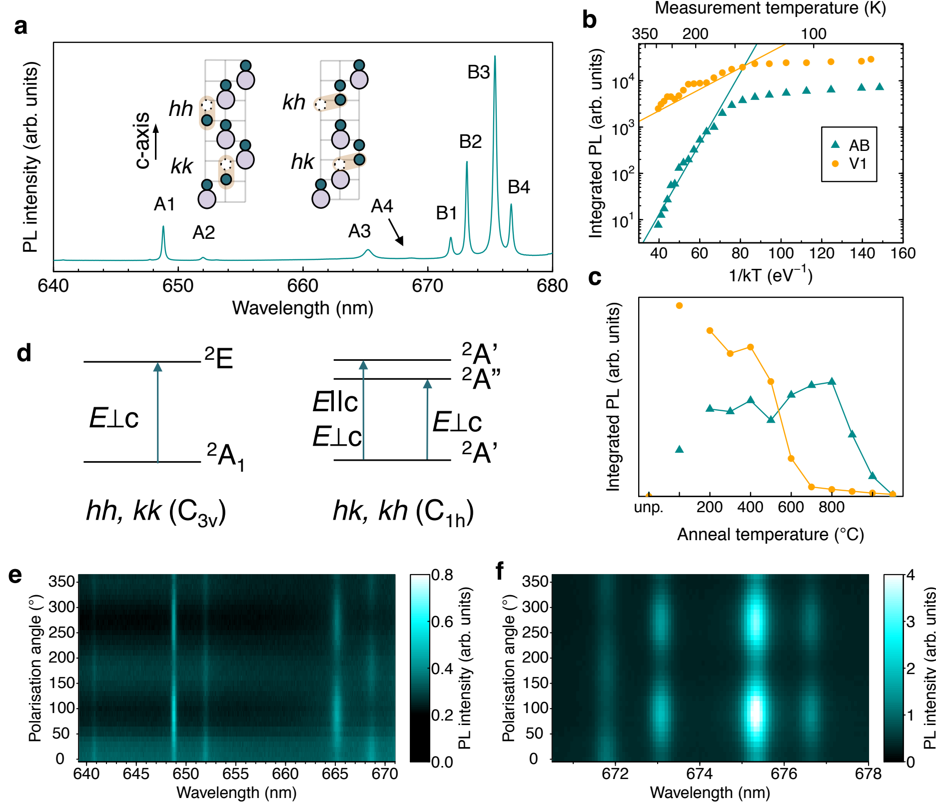

FIG. 1. **Ensemble measurements of defects in electron irradiated 4*H*-SiC.a,** The AB PL lines observed in an electron irradiated sample measured at 80 K. The proposed atomic structure of the defects, $C_{Si}V_C$, giving rise to the PL, are shown in the (1120) plane with the c-axis indicated in the inset (small and large circles represent C and Si atoms while the small open circles are vacancies). The carbon antisite-vacancy pair has four possible configurations in 4*H*-SiC: *hh*/*kk* axial configurations with C_{3v} symmetry, and *hk*/*kh* basal plane configurations with C_{1h} symmetry. *h* and *k* denote the hexagonal and cubic sites in the lattice, respectively. **b,** The temperature dependence of the AB and V1 PL lines and, **c,** their anneal temperature dependence. **d** Schematic diagram of the ground-state electronic structure of axial and basal plane configurations of the positively charged carbon antisite-vacancy defect. The symmetry labels of the defect states are depicted for each configuration. Arrows represent the feasible optical transitions with the corresponding polarization of light. **e,f,** The emission polarization dependence of the AB lines with the excitation beam perpendicular to the c-axis and the polarization angle θ, with θ=0 parallel to the c-axis.

electronic structure for both axial (*hh* and *kk*) and basal plane (*hk* and *kh*) configurations is

shown in Fig. 1d. These levels arise in the band gap due to the dangling bonds of the carbon antisite as well as of the Si-atoms nearest to the vacancy. In the axial configurations (C_{3v} symmetry) the lowest level has $^2A_1$ symmetry while the higher one has doubly degenerate ^2E symmetry. In the basal-plane configurations the double degenerate E state splits due to its lower C_{1h} symmetry.

Our ab-initio calculations indicate that the neutral $C_{Si}V_C$ pair does not have PL in the visible, in contrast to the previous assignment[27]. Thus, our working model is the positively charged $C_{Si}V_C$ pair with predicted visible PL. In the ground state only the lowest defect level is occupied by a single electron forming a totally symmetric state. The ^2E excited state of the axial configurations is subject to Jahn-Teller distortion while the basal configurations have *per se* C_{1h} symmetry. Thus, all the configurations may have low symmetry in their excited state, and the resulting many-body wave functions could have either $^2A''$ or $^2A'$ symmetry. The latter may partially borrow the character of the ground state due to sharing the same symmetry. The eight AB PL lines in 4H-SiC can naturally account for the four ground state configurations where each possesses two ZPLs. It was indeed shown that B_1 and B_3 lines are the higher excited states of B_2 and B_4 counterparts[27] separated by about 4 meV. A_1 and A_2 can naturally be grouped as well as the newly found A_3 and A_4 states, as they are separated by about the same energy as B_1 and B_3, or B_2 and B_4.

All the configurations can be efficiently excited by $E \perp c$ light while $E||c$ light only excites configurations to the A' excited state that partially shows the character of the ground state (Fig. 1d). Decay from the excited state can be more complicated than the optical excitation process. Direct recombination from the A'' or A' excited states to the A' (or A_1) ground state is possible with the same polarization dependence as in the absorption process. However, non-radiative decay from the ^2E-like excited state may occur through a ^4E-like shelving state with the aid of a spin-orbit interaction and vibrations. From the ab-initio calculations we conclude that only the single electron occupies the defect levels in the gap in the positively charged defect, thus a ^4E-like shelving state may form with a hole left in the valence band edge while the A_1 level and the split E level are occupied by a single electron.

The emission polarization of the $C_{Si}V_C$ lines at 80 K are shown in Fig. 1(e,f). Here, θ=0 corresponds to polarization parallel to the c-axis. We find that the lowest excitations of the two configurations (A_2 and A_4) are partially $E||c$ polarized while their higher energy counterparts, A_1 and A_3, are dominantly $E \perp c$ polarized. The other two configurations

with the lowest energy (B_2 and B_4) are also dominantly $E \perp c$ polarized. However, only B_1 shows partial parallel $E||c$ polarization, whereas B_3 is again dominantly $E \perp c$ polarized. This implies that the ground state character has only a minute contribution to the A' excited state in the B_4 defect. Our ab-initio calculations tentatively associate A_2, A_4, B_2 and B_4 lines with hh,hk,kk, and kh configurations, respectively.

To isolate single bright defect centers we performed PL raster scans on samples irradiated with a low electron fluence (1×10^{13} e/cm^2) using room temperature confocal microscopy. Typical maps are shown in Figure 2a,b obtained by exciting either with 532 or 660 nm light in the same area in the sample. The observed centers are found 1–1.5 μm below the surface (see Supplementary) which is amenable for the integration of these defects into on-chip optical waveguides in photonic circuits. The number of centers in these maps are shown in Fig. 2c as a function of their spatial diameter at half maximum. These are compared with an untreated sample excited with the 660 nm laser which also contains a number of optically-active centers but at a much reduced density. It is clear that the 532 nm excitation allows a larger number of centers to be addressed with both A and B lines being excited. The 660 nm laser will mostly excite only the B lines. Furthermore, although these sources are present in these particular untreated samples, irradiation and annealing significantly increase their density (Fig.2d) (see Supplementary) similar to the ensemble measurements presented above.

PL spectra corresponding to the bright spots in the confocal maps, when excited using either 660 or 532 nm are shown in Fig. 2e. We find that all the measured diffraction limited spots of 300-400 nm in diameter have PL emission between 675 to 700 nm, when excited at 660 nm, or with broader emission with peaks from $\sim$660 nm to $\sim$705 nm when excited at 532 nm. Such emission corresponds to that of the room temperature PL of the AB lines. We therefore identify the defect responsible for this emission with the $C_{Si}V_C$ pair. Some variability is observed in the PL peak position (see Supplementary) possibly as a result of addressing defects of a specific configuration.

To confirm that single defects are being addressed, a Hanbury-Brown and Twiss interferometer was used to verify single photon emission. We observed that all defects displaying PL between 648–710 nm behaved as single photon sources, i.e. the second order photon correlation function at zero delay is $g^{(2)}(0) < 0.5$ (Fig. 2 f). We analyzed $g^{(2)}(\tau)$ at different excitation powers to study the photo-physics and the population dynamics from the ground

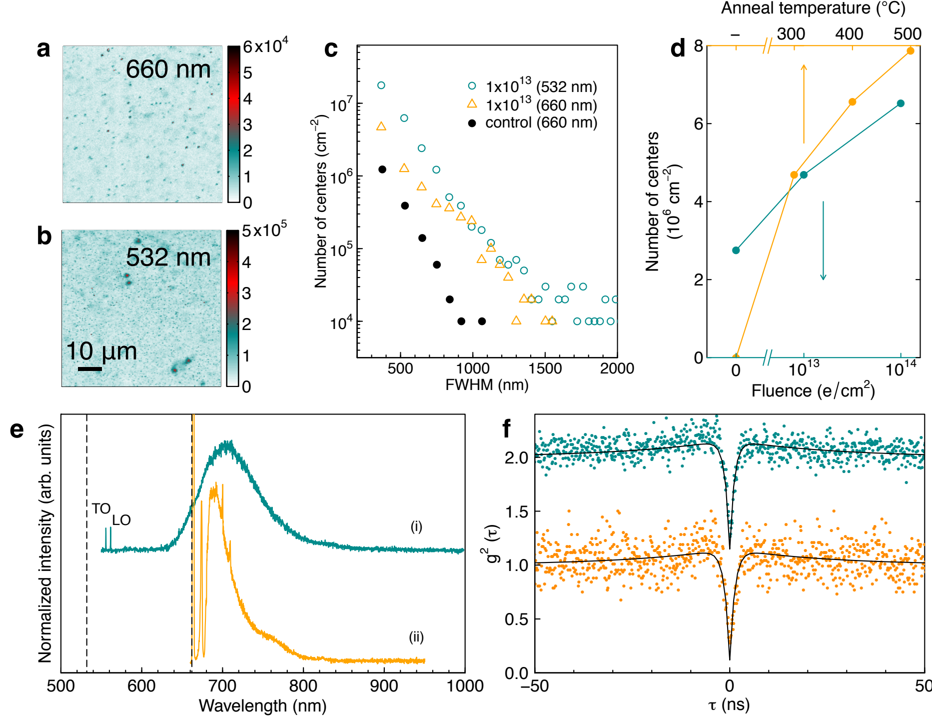

FIG. 2. **Confocal microscopy Single defects localization in** $4H$**-SiC.** Confocal map of the low electron fluence sample excited with 660 nm (**a**) and 532 nm (**b**) lasers. The diffraction limited spots all correspond to single photon emitters. Map (a) has been scanned using a 10 nm FWHM 694 nm filter. Note the difference in color scale. **c,** Histogram of the number of centers observed as a function of the spatial FWHM measured and counted from **a,b**. The histogram from a confocal map of an unprocessed sample is also shown indicating a clear increase in the defect density after irradiation and annealing at 300°C. **d** The number of diffraction limited optical centers measured from single defects as a function of the anneal temperature (top axis) and fluence (bottom axis) **e,** Normalized room temperature PL of a single photon source in the irradiated sample excited with 532 nm (i) and 660 nm (ii,iii) lasers. The laser wavelengths are indicated by the dashed lines. The transverse and longitudinal optic Raman modes (TO, LO) are also indicated. **f,** The corresponding anti-bunching curves for **e**(i) and (ii).

state to the excited state. To assess the properties of the single photon emission accurately, the variability of their kinetics was established. Many photo-stable emitters (more than 100) were measured with the two different excitation wavelengths and analyzed. From this analysis we deduced a typical excited state lifetime of 1.2 ns, the existence of a metastable state with a short life time and a quantum efficiency of the defect of 70%. The shelving

state is predicted by our theoretical model and is an intrinsic part of the center's electronic structure. The observed short metastable state lifetime can be due to effective scattering from the sub-states of the shelving state.

The saturation properties of the defects also display a remarkable variability, with optical saturation powers observed between 0.2 to 3.3 mW and saturation count rates found from 2.5×10^5 counts/s to the maximum observed of 2×10^6 counts/s. This variability is associated with the metastable state lifetime variation. The high quantum efficiency and the most efficient excitation of axial defects (excitation orthogonal to the c-axis) allows the maximum collection efficiency with the optical configuration of the confocal system used, yielding the high count rate measured for this defect.

We monitored the PL emission stability of these defects in a sample irradiated and annealed at 300°C. It was observed that 45% of the emitters measured were stable over a long period of time. An example of such a single center is shown in Fig. 3a along with its associated Gaussian count rate histogram in Fig. 3b. Interestingly, the remaining centers showed PL blinking with some eventually photo-bleaching, even if not permanently. Blinking centers in samples annealed at higher temperatures (500°C) were almost absent even though the single photon source density was greater. By annealing up to 800 °C 65% of the emitter were stable for days at 532 nm excitation.

This suggests that the photo-stability may be compromised by the density of non-radiative pathways which are thermally unstable and annihilate on annealing. An emitter with on-off fluorescence, between two PL states is shown in Fig. 3c,d. By measuring all on/off-time durations in a single trace, the corresponding probability of occurrence $P(\tau_{on,off})$ can be calculated. The distribution of the "on" and "off" times are plotted on a semi-logarithmic scale in Fig.3e together with the fits. Both $P(\tau_{on})$ and $P(\tau_{off})$ show an exponential trend following the equation:

$$P(\tau_{on,off}) \propto \exp[-\tau/(\tau_{on,off})] \quad (1)$$

with the time constant, τ_{on} usually much greater than τ_{off} (Fig. 3f) and very sensitive to the excitation power. This is in contrast to the more common power law dependence usually observed for blinking. We attribute the observed blinking to either a photo-induced charge conversion of the addressed defect or to a charge exchange with other defects in close proximity, acting as charge traps or donors, likely induced by irradiation. Samples annealed

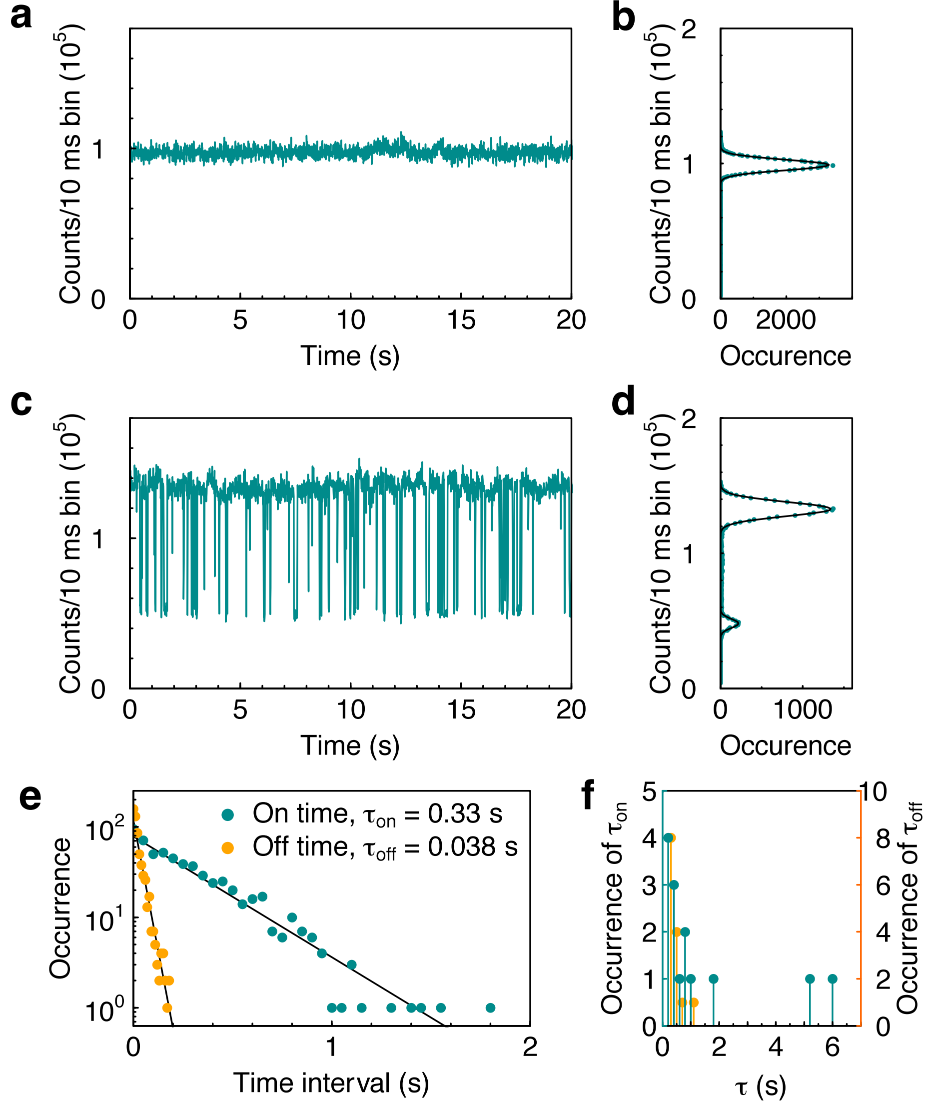

FIG. 3. **Photo-stability of single photon sources in SiC. a**, 20 s fragment of a PL time-trace sampled into 10 ms bins from a stable single photon source with its corresponding count rate histogram (**b**). **c,d**, A similar time trace is shown for a blinking center. The on and off times of (**b**) on a semi-logarithmic scale. **f,** Histogram of the measured τ_{on} and τ_{off} of the 55 emitters analyzed. 45% of the emitters in this sample were stable and did not show blinking behavior.

at higher temperature revealed a largely reduced number of blinking defects, indicating that the blinking can be controlled. In addition, the defects were more stable using 660 nm excitation.

Our atomistic model of the defect (see Supplementary) indicates that the nature of the shelving state may also be responsible for the blinking properties (e.g., a nearby defect can

effectively capture the loosely bound hole and hinder the luminescence). This is consistent with our observation that with the appropriate anneal the defect density is reduced and blinking is minimized. Blinking may also arise in our working model by the fact that if the defect was originally neutral then it can be efficiently ionized to the luminescent positively charge state; in this case the electrons should be continuously pumped to the conduction band in order to maintain the luminescence; 660 nm excitation can ionize the neutral defect but it has less probability to ionize the defect further (doubly positive charge state), thus it can show greater photo-stability than with 532 nm excitation. Given that the blinking can be controlled with either laser power, wavelength and annealing, we conclude that blinking is not an intrinsic property of the defect.

In our working model the spin state is 1/2 for the positively charged $C_{Si}V_C$ defect. Clearly, further theoretical modelling and experiments are required to determine if this charge state could have a optically detected magnetic resonance (ODMR). We note that our working model indicates a relatively low ODMR signal because its metastable shelving state has low symmetry with a strong mixture of $m_S = \pm 1/2$ and $m_S = \pm 3/2$ substates. With a small magnetic field the ground state can be split but it is not understood whether different decay rates to these two states will be different enough to observe ODMR. The metastable state however might be used for spin readout. We further note that spin-1/2 $C_{Si}V_C$ defect may cause decoherence of silicon-vacancy spins where silicon-vacancy is created with optically polarizable spins together with $C_{Si}V_C$ defect. The $C_{Si}V_C$ spin may communicate with silicon-vacancy spins via dipole-dipole interaction which affects the coherence time of those spins[20,29]. Thus, the manipulation of the ground and excited states of $C_{Si}V_C$ defect at single defect level might be useful in the manipulation of the other proximate spins in SiC that can be addressed optically.

In conclusion, this ultra-bright single photon emitter working at room temperature provides a new building block in SiC-based opto-electronic devices and future integrated quantum photonics[9]. We envisage that SiC will constitute an ideal platform for future integrated photonic circuits comprising photonic cavities and waveguides, presently under fabrication. Our defect assignment yields good agreement with observations. The counterparts to this intrinsic defect can exist in other SiC polytypes and may also possess single photon emission characteristics. The incorporation of these bright defects in SiC nanoparticles and SiC quantum dots could provide an exciting opportunity for biological imaging and microscopy.

Further optimization of the defect formation and excitation is expected to improve the photo-stability, its brightness and understanding of its properties. Electrical excitation of the center is also a very realistic possibility which may result in SiC-LEDs with active quantum systems[31].

METHODS

Sample preparation

The material under study is high purity semi-insulating (HPSI) 4*H*-SiC purchased from CREE. According to the manufacturer, the as-received samples contained B (10^{14} cm^{-3}), C interstitials (10^{14} cm^{-3}) and N ($<10^{14}$ cm^{-3}).

Samples were irradiated with 2 MeV electrons to fluences of 1×10^{13}, 1×10^{15} and $1\times^{17}$ e/cm^2 at a flux of 2.82×10^{12} cm^{-2}s^{-1}. The samples were held at temperatures below 80°C during irradiation in a nitrogen ambient to inhibit Frenkel pair annihilation and reduce the possibility of contamination. After irradiation, a low temperature (300°C) anneal in an Ar ambient for 30 minutes was performed. This temperature was chosen so as to enhance the concentration of various defects of interest based on ensemble electron spin resonance (ESR) measurements[32]. An unprocessed sample from the same wafer was also characterized in order to establish the effectiveness of the irradiation procedure employed.

Similar samples were also annealed for 30 minutes at 300, 400, 500, 800°C in an Ar ambient after 2 MeV electron irradiation to a fluence of 10^{13} e/cm^2.

Photoluminescence and photon correlation measurements

A Hanbury-Brown-Twiss interferometer was used to identify optically active single defects and measure the time correlation of the center emission. In the confocal microscope the samples were excited using 0.2-1.5 mW continuous wave laser operating at 532 nm (Coherent, model: Compass 315M-100) and continuous diode laser operating at 665 nm. The laser was focused onto the sample using a 100x infinity-corrected oil immersion objective lens with a NA of 1.4 and the luminescence was collected confocally through a 50 μm pinhole. A spectrometer (Princeton Instruments Acton 2500i, Acton) with a cooled CCD (Camera Pixis 100 model: 7515-0001 Princeton Instruments) was used to characterize the luminescence

and a HBT interferometer with single-photon-sensitive avalanche photodiodes (Perkin Elmer SPCM-AQR 14) was used to measure the photon statistics. Photon counting and correlation was carried out using a time-correlated single-photon-counting (TCSPC) module (PicoHarp 300, PicoQuant GmbH).

The 4H SiC samples were mounted on a piezo XYZ stage allowing 100x100 μm^2 scans. The unwanted residual laser line was eliminated by a 660 nm long pass filter. A filter with 694±10 nm was placed in front of HBT interferometer to observe single photons during 660 nm laser excitation. The spectroscopy was done using only a long pass filter. All the single photon/single defect measurements were performed at room temperature.

A Renishaw MicroRaman Spectrometer equipped with a Linkam stage for temperature control was used for the ensemble PL measurements. A 532 nm laser was directed through a 20x long working distance objective with a 0.4 NA onto the sample. The laser power at the sample was approximately 0.5 mW. The spectrometer has a working distance of 0.25m and uses an 8 μm slit and a 1200 g/mm grating. The detector is a fan cooled Si CCD.

Atomistic simulations

Theoretical calculations were carried out using density functional theory and group theory. A 576-atom supercell with Γ-point sampling of the Brillouin-zone was used in the supercell calculations on the $C_{Si}V_C$ defects in 4*H*-SiC. A Γ-point calculation is sufficient to provide convergent charge density and enabled us to study the degeneracy of the defect levels. We applied HSE06 hybrid DFT which is able to reproduce the experimental band gap of 4*H*-SiC ($\approx$ 3.2 eV) and defect levels in the fundamental band gap[33,34]. We note that we were able to identify the electron paramagnetic (EPR) spectrum of the negatively charged and positively charged $C_{Si}V_C$ pair using supercell DFT methods in 32 and 35.

---

* stefania.castelletto@rmit.edu.au

1 Basché, T., Moerner, W. E., Orrit, M. & Talon, H. Photon antibunching in the fluorescence of a single dye molecule trapped in a solid. *Phys. Rev. Lett.* **69**, 1516–1519 (1992).

2 Michler, P. *et al.* Quantum correlation among photons from a single quantum dot at room temperature. *Nature* **406**, 968–970 (2000).

[3] Santori, C., Fattal, D., Vuckovic, J., Solomon, G. S. & Yamamoto, Y. Indistinguishable photons from a single-photon device. *Nature* **419**, 594–597 (2002).

[4] Shields, A. J. Semiconductor quantum light sources. *Nat. Photonics* **1**, 215–223 (2007).

[5] Kurtsiefer, C., Mayer, S., Zarda, P. & Weinfurter, H. Stable solid-state source of single photons. *Phys. Rev. Lett.* **85**, 290–293 (2000).

[6] Kolesov, R. *et al.* Optical detection of a single rare-earth ion in a crystal. *Nat Commun* **3**, 1029– (2012).

[7] Peruzzo, A., Shadbolt, P., Brunner, N., Popescu, S. & O'Brien, J. L. A quantum delayed-choice experiment. *Science* **338**, 634–637 (2012).

[8] Lundeen, J. S., Sutherland, B., Patel, A., Stewart, C. & Bamber, C. Direct measurement of the quantum wavefunction. *Nature* **474**, 188–191 (2011).

[9] Politi, A., Matthews, J. C. F. & O'Brien, J. L. Shor's quantum factoring algorithm on a photonic chip. *Science* **325**, 1221 (2009).

[10] Yamada, S., Song, B.-S., Asano, T. & Noda, S. Silicon carbide-based photonic crystal nanocavities for ultra-broadband operation from infrared to visible wavelengths. *Appl. Phys. Lett.* **99**, 201102 (2011).

[11] Madar, R. Materials science: Silicon carbide in contention. *Nature* **430**, 974–975 (2004).

[12] Nakamur, D. *et al.* Ultrahigh-quality silicon carbide single crystals. *Nature* **430**, 1009–1012 (2004).

[13] Lu, X., Lee, J. Y., Feng, P. X.-L. & Lin, Q. Silicon carbide microdisk resonator. *Opt. Lett.* **38**, 1304–1306 (2013).

[14] Fan, J. *et al.* 3C-SiC nanocrystals as fluorescent biological labels. *Small* **4**, 1058–1062 (2008).

[15] Beke, D. *et al.* Silicon carbide quantum dots for bioimaging. *J. Mater. Res.* **28**, 205–209 (2013).

[16] Gali, A. Excitation spectrum of point defects in semiconductors studied by time-dependent density functional theory. *J. Mater. Res.* **27**, 897–909 (2012).

[17] Weber, J. R. *et al.* Quantum computing with defects. *Proc. Natl Acad. Sci.* **107**, 8513–8518 (2010).

[18] Koehl, W. F., Buckley, B. B., Heremans, F. J., Calusine, G. & Awschalow, D. D. Room temperature coherent control of defect spin qubits in silicon carbide. *Nature* **479**, 84 (2011).

[19] Baranov, P. G. *et al.* Silicon vacancy in SiC as a promising quantum system for single-defect and single-photon spectroscopy. *Phys. Rev. B* **83**, 125203 (2011).

[20] Falk, A. L. *et al.* Polytype control of spin qubits in silicon carbide. *Nat. Commun.* **4**, 1819 (2013).

[21] DiVincenzo, D. Quantum bits: Better than excellent. *Nat. Mater.* **9**, 468–469 (2010).

[22] Aharonovich, I. *et al.* Chromium single-photon emitters in diamond fabricated by ion implantation. *Phys. Rev. B* **81**, 121201 (2010).

[23] Aharonovich, I. *et al.* Two-level ultrabright single photon emission from diamond nanocrystals. *Nano Letters* **9**, 3191–3195 (2009).

[24] Neu, E. *et al.* Single photon emission from silicon-vacancy colour centres in chemical vapour deposition nano-diamonds on iridium. *New J. Phys.* **13**, 025012 (2011).

[25] Schröder, T., Gädeke, F., Banholzer, M. J. & Benson, O. Ultrabright and efficient single-photon generation based on nitrogen-vacancy centres in nanodiamonds on a solid immersion lens. *New J. Phys.* **13**, 055017 (2011).

[26] Ates, S. *et al.* Improving the performance of bright quantum dot single photon sources using temporal filtering via amplitude modulation. *Sci. Rep.* **3** (2013).

[27] Steeds, J. W. Photoluminescence study of the carbon antisite-vacancy pair in 4H- and 6H-SiC. *Phys. Rev. B* **80**, 245202 (2009).

[28] Steeds, J. *et al.* Transmission electron microscope radiation damage of 4H and 6H SiC studied by photoluminescence spectroscopy. *Diamond Relat. Mater.* **11**, 1923–1945 (2002).

[29] Soltamov, V. A., Soltamova, A. A., Baranov, P. G. & Proskuryakov, I. I. Room temperature coherent spin alignment of silicon vacancies in 4H- and 6H-SiC. *Phys. Rev. Lett.* **108**, 226402 (2012).

[30] Bockstedte, M., Mattausch, A. & Pankratov, O. *Ab initio* study of the annealing of vacancies and interstitials in cubic SiC: Vacancy-interstitial recombination and aggregation of carbon interstitials. *Phys. Rev. B* **69**, 235202 (2004).

[31] Fuchs, F. *et al.* Silicon carbide light-emitting diode as a prospective room temperature source for single photons. *Sci. Rep.* **3**, 1637 (2013).

[32] Umeda, T. *et al.* Identification of the carbon antisite-vacancy pair in 4H-SiC. *Phys. Rev. Lett.* **96**, 145501 (2006).

[33] Deák, P., Aradi, B., Frauenheim, T., Janzén, E. & Gali, A. Accurate defect levels obtained from the HSE06 range-separated hybrid functional. *Phys. Rev. B* **81**, 153203 (2010).

[34] Ivády, V., Gällström, A., Son, N. T., Janzén, E. & Gali, A. Asymmetric split-vacancy defects in SiC polytypes: A combined theoretical and electron spin resonance study. *Phys. Rev. Lett.* **107**, 195501 (2011).

[35] Umeda, T. *et al.* Identification of positively charged carbon antisite-vacancy pairs in 4H-SiC. *Phys. Rev. B* **75**, 245202 (2007).

SUPPLEMENTARY INFORMATION

Supplementary information is linked to the online version of the paper at www.nature.com/nmat.

ACKNOWLEDGEMENTS

S.C. acknowledges the funding support from the Australian Research Council, Centre of Excellence Engineered Quantum Systems (CE110001013). B.C.J. acknowledges financial support from the Japanese Society for the Promotion of Science (JSPS) (Grant-in-aid for Scientific Research, 22.00802) and the Australian Research Council Centre for Quantum Computation and Communication Technology (CE110001027). This study is also partially supported by the Ministry of Education, Science, Sports and Culture, Grant-in-Aid for Challenging Exploratory Research, 2012, 24656025. A.G. acknowledges the EU FP7 Grant No. 270197 (DIAMANT), the Hungarian OTKA Grant No. K101819 and K106114, as well as the support from Knut and Alice Wallenberg Foundation.

AUTHOR CONTRIBUTIONS

SC and BCJ proposed the idea and the strategy for the experimental design and data analysis and wrote the paper. SC performed the optical single photon characterization experiments. BCJ irradiated and annealed the samples. NS performed some of the low temperature PL measurements. SC and BCJ coordinated the experiments and analyzed the data. VI and AG performed the theoretical model of the center. SC, BCJ and AG contributed to write the manuscript. All authors discussed the results and commented on the manuscript.

AUTHOR INFORMATION

Reprints and permissions information is available at www.nature.com/reprints. The authors declare no competing financial interests. Supplementary information accompanies this paper. Readers are welcome to comment on the online version of this article at www.nature.com/nmat. Correspondence and requests for materials should be addressed to S.C (stefania.castelletto@rmit.edu.au).